Matter density distributions of ^{20,22}Ne and ^{24,26}Mg extracted through proton elastic scattering at 0.8 GeV

Z. H. Li [1,2,3] Y. Kuang,[4] Y. Huang,[3,5] X. L. Tu [3,6,*] Z. P. Li [5] K. H. Fang,[2] J. T. Zhang,[1,2,3] and K. Yue[3,6]

[1]*Joint Department for Nuclear Physics, Institute of Modern Physics, Chinese Academy of Sciences and Lanzhou University, Lanzhou 730000, China*

[2]*School of Nuclear Science and Technology, Lanzhou University, Lanzhou 730000, China*

[3]*Institute of Modern Physics, Chinese Academy of Sciences, Lanzhou 730000, China*

[4]*School of Physical Science and Technology, Southwest University, Chongqing 400715, China*

[5]*Key Laboratory of Radiation Physics and Technology of the Ministry of Education, Sichuan University, Chengdu 610064, China*

[6]*School of Nuclear Science and Technology, University of Chinese Academy of Sciences, Beijing 100049, China*

Reported small-angle differential cross sections of proton elastic scattering off ^{20,22}Ne and ^{24,26}Mg at 0.8 GeV were analyzed with the Glauber model. Matter density distributions of ^{20,22}Ne and ^{24,26}Mg were determined based on the two-parameter Fermi density model, and the corresponding root-mean-square point-matter radii are 2.891(52) fm, 2.895(104) fm, 2.935(20) fm, and 2.946(21) fm. The occupation number effects of the $2s$ orbital on inner density were probed by the matter density difference between ^{22}Ne and ^{24}Mg. Combined with the experimental occupation numbers, the relativistic Hartree-Bogoliubov calculations with the DD-ME2 and PC-PK1 interactions describe the obtained density difference trend, and indicate that there may be a bubble structure in ^{24}Mg.

I. INTRODUCTION

Atomic nuclei are quantum many-body systems consisting of interacting neutrons and protons. Radial density distributions of the constituent nucleons are one of the most fundamental properties of atomic nuclei. The root-mean-square (rms) radii reflecting the size of nuclei are related to the density distributions. They play an extremely important role in nuclear structure and astrophysics investigations [1–7]. The small difference of neutron and proton radii in a nucleus, known as the halo and skin phenomena [8], has a direct relationship with the large neutron star radius [9]. Furthermore, the density distribution difference of neighboring nuclei is also a sensitive tool for probing occupation number and radial wave function in single-particle orbital via $\delta\rho(r) = \sum \delta n_{nlj}|R(r)_{nlj}|^2$ [10–17], where n_{nlj} and $R(r)_{nlj}$ are the occupation number and the radial wave function for each orbital, respectively. For example, the radial wave function for the $3s$ orbital was determined by the charge density difference between ^{206}Pb and ^{205}Ti [12].

The single-particle radial density distributions for the s orbitals have a common character, that is to say, there are density peaks in the center of nuclei [12]. So the occupation numbers of the s orbitals are essential to understand the anomalous low densities in the interior of nuclei [18–24]. The low densities are known as the bubble structure, and were first raised by Wilson in 1946 [25]. In the sd shell,

for instance, ^{34}Si [18,19,26] and ^{46}Ar [23] were expected to have the bubble structures. But as authors in Ref. [24] concluded that it is difficult to make a reliable prediction, due to the unknown single-particle information. The deformed Ne and Mg isotopes in the middle sd shell were widely investigated [22,27–31]. The obtained nucleon occupation numbers of 1.5 for the $2s$ orbital were reduced to about 0.34 from ^{22}Ne to ^{24}Mg by adding two valence protons [22]. This would result in a decreasing of the inner matter density, as a result, a bubble structure in ^{24}Mg may be formed.

Experimentally, matter density distributions in nuclei can be also precisely extracted from such as interaction cross sections [8,32,33] and hadron-scattering cross sections [11,34–36] based on reaction models, although the model-independent parity violating electron nucleus scattering has been developed to measure the spatial distributions of neutrons in nuclei [37]. For example, the matter radii of the Ne and Mg isotopes were extracted through the interaction cross sections [32,33]. As known, the small-angle differential cross sections of proton-nucleus elastic scattering are from peripheral collisions, and are sensitive to surface matter density distributions. Especially, thanks to the high reaction cross sections, the small-angle elastic scatterings can be precisely measured. Consequently, different facilities, such as the hydrogen-filled ionization chamber IKAR [2,38,39] and the in-ring reaction facility (IRRF) based internal gas-jet target [11,36,40–43] were developed to measure the small-angle elastic scattering differential cross sections for matter density distribution determinations.

———————
*tuxiaolin@impcas.ac.cn

Precise determination of inner density distribution is difficult [12]. However, the inner density difference of neighboring nuclei can be touched by the surface density according to the nucleon number conservation. Recently, a significant inner core rearrangement effect from ^{56}Ni to ^{58}Ni was found via their surface matter density distributions, which were determined by the small-angle differential cross sections of proton-nucleus elastic scattering [11]. To study the influence of occupation numbers on density distributions, we extracted the matter density distributions of ^{20,22}Ne and ^{24,26}Mg from the small-angle differential cross sections of proton-nucleus elastic scattering in this work. These data would be helpful to clarify the mentioned radius inconsistency for ^{22}Na [44].

II. DETERMINATION OF MATTER DENSITY DISTRIBUTION

The used experimental differential cross sections of proton elastic scattering off ^{20,22}Ne and ^{24,26}Mg at 0.8 GeV were taken from the EXFOR database [45]. They were measured at the high resolution spectrometer (HRS) at the Clinton P. Anderson Meson Physics Facility (LAMPF) of the Los Alamos Scientific Laboratory [30,31]. Compared to the absolute normalization uncertainties of about 10%, a relative precision of about 1% was achieved for the small-angle differential cross sections. More details on experiments can be found in Refs. [30,31].

Proton-nucleus elastic scatterings can provide useful information on matter density distributions in nuclei through appropriate reaction models [35,46]. To extract matter density distributions, following the methods in Refs. [11,38,39], the small-angle differential cross sections were fitted by a procedure based on the Glauber multiple-scattering theory [47] in this work. More details on the Glauber procedure can be found in Refs. [39,46] and references cited therein. The differential cross sections of proton-nucleus elastic scattering were calculated in the Glauber model via [39]

$$\frac{d\sigma}{d\Omega}(\theta) = |F_{\text{el}}(\boldsymbol{q})|^2 \quad , \tag{1}$$

where the elastic scattering amplitude $F_{el}(\boldsymbol{q})$ is a function of the matter density $\rho(r)$ and the proton-nucleon (pN) profile function γ_{pN}. The γ_{pN} is related to the free pN scattering amplitude $f_{pN}(q)$ as

$$\gamma_{pN}(\boldsymbol{b}) = \frac{1}{2\pi i k} \int \exp(-i\boldsymbol{q}\boldsymbol{b}) f_{pN}(\boldsymbol{q}) d^2\boldsymbol{q} \quad . \tag{2}$$

As known, the effects of the spin-orbit can be neglected in the small-angle region [46]. Thus, the calculations of the scattering amplitude in the Glauber model can be performed with less parameters. Only the scalar parts of the pN scattering amplitudes were taken into account, the $f_{pN}(\boldsymbol{q})$ was calculated by the standard high-energy parametrization as

$$f_{pN}(\boldsymbol{q}) = \frac{ik}{4\pi} \sigma_{pN}(1 - i\alpha_{pN})\exp\left(\frac{-\boldsymbol{q}^2\beta_{pN}}{2}\right) \quad , \tag{3}$$

where σ_{pN}, α_{pN}, and β_{pN} are the total cross sections, ratios of the real to imaginary parts of the forward-scattering amplitudes, and slope parameters for proton-proton (pp) and

TABLE I. The obtained R, a, and rms point-matter radii R_m for ^{20,22}Ne and ^{24,26}Mg in this work. The reported matter radii R_m^{lit} [33] are also listed. The errors in parentheses are only statistical uncertainties.

Nucleus	R (fm)	a (fm)	R_m (fm)	R_m^{lit} (fm)
^{20}Ne	2.422(67)	0.592(30)	2.891(52)	2.870(30) [33]
^{22}Ne	2.396(170)	0.598(66)	2.895(104)	
^{24}Mg	2.860(55)	0.518(21)	2.935(20)	2.790(150) [33]
^{26}Mg	2.904(57)	0.512(22)	2.946(21)	2.990(40) [27]

proton-neutron (pn) channels, respectively. We noted that different α and β values were once used to describe the proton-nucleus elastic scattering differential cross sections at 0.8 GeV [13,14]. The σ_{pN} and α_{pN} in the energy range from about 0.4 GeV to 1 GeV were evaluated in Ref. [39]. The reliability of these data at $\approx$700 MeV have been verified [38,39]. In this work, the adopted values were taken from Refs. [39,48], where $\sigma_{pp} = 4.70(2)$ fm^2, $\sigma_{pn} = 3.80(2)$ fm^2, $\alpha_{pp} = -0.02(6)$, $\alpha_{pn} = -0.34(6)$, and $\beta_{pp} = \beta_{pn} = 0.20(5)$ fm^2. The errors are standard deviations of the reported data in Refs. [13,14,39,48,49].

Similar to the charge density distributions of ^{20,22}Ne and ^{24,26}Mg [50], we also used the two-parameter Fermi (2pF) model to describe the surface matter density distributions in the present work,

$$\rho(r) = \rho(0) \frac{1}{1 + \exp\left(\frac{r-R}{a}\right)} \quad , \tag{4}$$

where $\rho(0)$ is the density normalization factor. R and a are the half-density radius and the diffuseness parameter, respectively.

The absolute normalization uncertainties for the used differential cross sections are relatively large. To reduce the effects of the normalization uncertainties, the matter density distributions were extracted by fitting relative differential cross sections $\frac{d\sigma}{d\Omega}(\theta)_{re}$. This method has been used to determine the matter radius of ^{16}O [51]. Consequently, in the χ^2-fit procedure, R, a, and cross section normalization parameter L_0 were used as free parameters, and adjusted to make χ^2 achieve minimum. The matter density distributions $\rho(r)$ were determined by the obtained R and a. Subsequently, the rms matter radii can be calculated via $R_m = [\int \rho(r)r^4 dr / \int \rho(r)r^2 dr]^{1/2}$. The χ^2 function was defined as

$$\chi^2 = \sum_i^{N_0} \frac{\left[L_0 \frac{d\sigma}{d\Omega}(\theta_i)_{re} - \frac{d\sigma}{d\Omega}(\theta_i)_{\text{cal}}\right]^2}{\left[L_0 \Delta \frac{d\sigma}{d\Omega}(\theta_i)_{re}\right]^2} \quad , \tag{5}$$

where N_0 and $\Delta \frac{d\sigma}{d\Omega}(\theta)_{re}$ are the number of data points and the uncertainties of the measured differential cross sections, respectively. The $\frac{d\sigma}{d\Omega}(\theta)_{\text{cal}}$ are the differential cross sections calculated by the Glauber model.

Figure 1 shows the best fits for the relative differential cross sections as a function of scattering angle θ in the center-of-mass frame. The determined 2pF parameters and the rms point-matter radii for ^{20,22}Ne and ^{24,26}Mg are tabulated in Table I. Figures 2 and 3 show the obtained 2pF matter
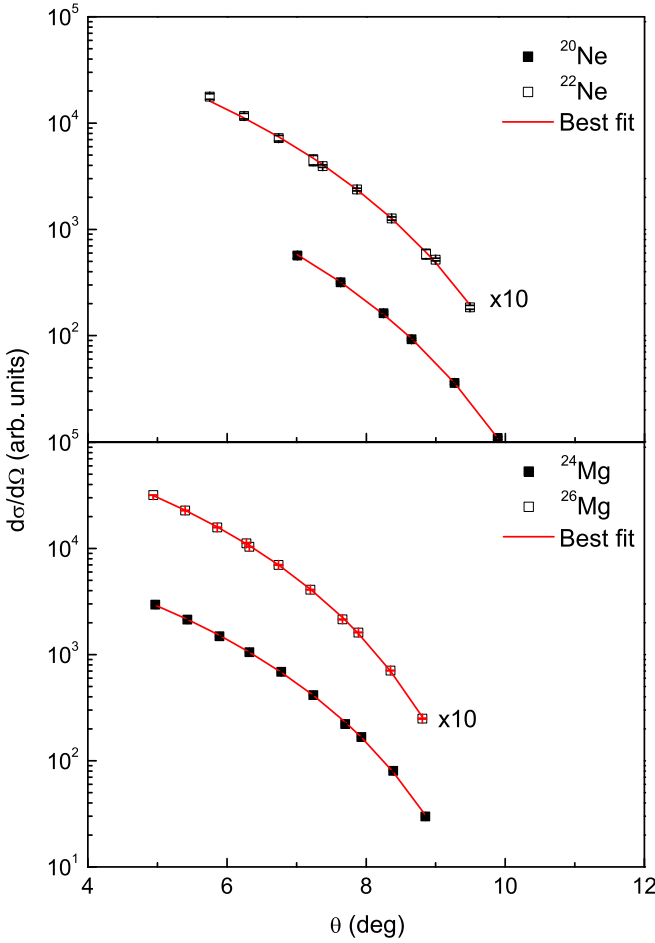
FIG. 1. The best fit of the relative differential cross sections as a function of scattering angle θ in the center-of-mass frame. The relative differential cross sections were normalized by multiplying with L_0 to the absolute cross sections calculated by the Glauber model.

density distributions for ^{22}Ne and ^{24}Mg. Statistical uncertainties were standard deviations of the corresponding data. These data were obtained by fitting hundreds of randomly sampling differential cross sections based on the Gaussian distribution within $\frac{d\sigma}{d\Omega}(\theta_i) \pm 2\Delta\frac{d\sigma}{d\Omega}(\theta_i)$. The errors of the experimental differential cross sections were scaled to make the normalized χ_n of the best fit equals 1. Uncertainties of the input parameters σ_{pN}, α_{pN}, and β_{pN} would result in systematic errors of about 0.08 fm, 0.05 fm, 0.03 fm, and 0.03 fm for ^{20}Ne, ^{22}Ne, ^{24}Mg, and ^{26}Mg, respectively.

III. DISCUSSION

The obtained matter radii in this work for ^{20}Ne and ^{24}Mg, respectively, are 2.891(52) fm and 2.935(20) fm. They are consistent with the results extracted through the interaction cross sections [32,33], see Table I. Otherwise, since ^{20}Ne and ^{24}Mg have equal neutron and proton numbers, their matter and proton radii would be almost identical. Our matter radii agree very well with the proton radii of 2.889 fm and 2.942 fm for ^{20}Ne and ^{24}Mg, which were deduced from the charge radii
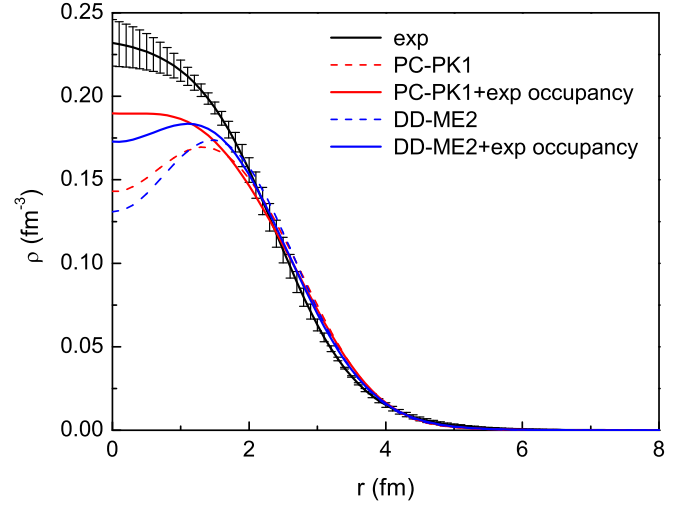

FIG. 2. Comparison of the obtained 2pF matter density distribution (black) and theoretical results for ^{22}Ne. Red and blue dashed lines denote the theoretical distributions calculated by the PC-PK1 and DD-ME2 interactions, respectively. Red and blue solid lines are for the PC-PK1 and DD-ME2 calculations with the experimental occupation numbers, respectively. The error bars are only statistical errors, which were caused by the statistical uncertainties of the experimental differential cross sections. The used small-angle differential cross sections are not sensitive to deriving experimentally the central density profiles.

via $R_p^2 = R_{ch}^2 - r_p^2 - \frac{N}{Z}r_n^2 - \frac{3\hbar^2}{4m_p^2c^2}$ [52]. The charge radius R_{ch}, proton charge radius r_p, and squared charge radius of neutron r_n^2 were taken from Ref. [53]. The Darwin-Foldy correction factor $\frac{3\hbar^2}{4m_p^2c^2}$ was 0.033 fm^2 [52]. These consistencies indicate a reliability of this work.

Compared to ^{20}Ne and ^{24}Mg, the reported matter radius of 2.720(40) fm for the neighboring self-conjugate nuclei ^{22}Na [32,33] is smaller than by about 0.2 fm. This large deviation is not observed by the systematic trend of the charge radii [53],
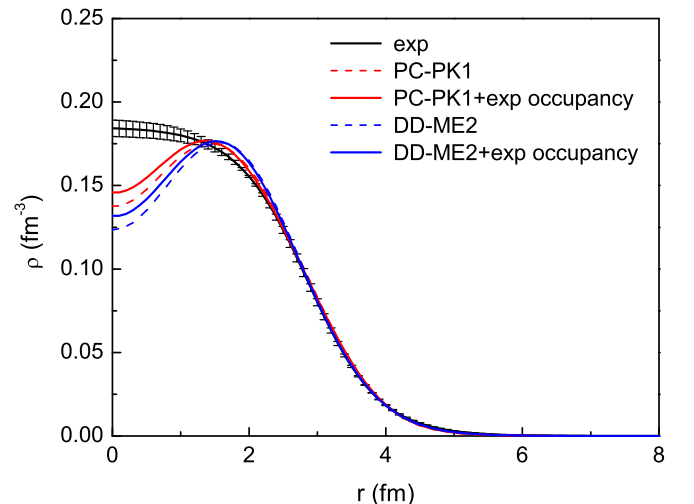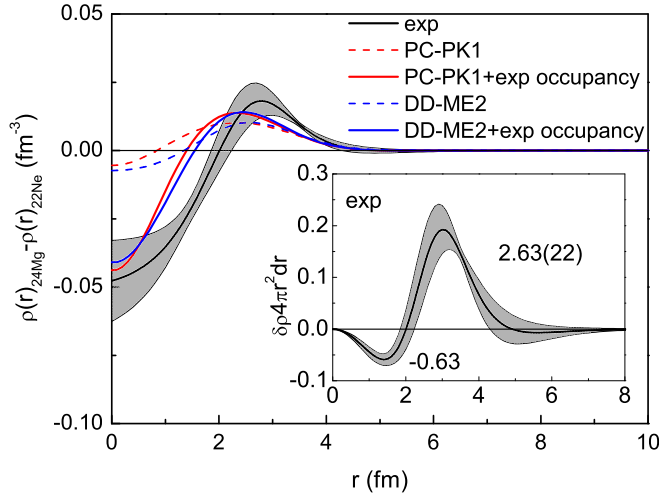

FIG. 3. Same as Fig. 2, but for ^{24}Mg.

FIG. 4. Density distribution difference between ^{22}Ne and ^{24}Mg, which was obtained based on the 2pF density model. The insert shows the rearrangement of nucleons from ^{22}Ne to ^{24}Mg deduced by their density difference, where dr is 0.1 fm. Red and blue dashed lines denote the theoretical distributions calculated by the PC-PK1 and DD-ME2 interactions, respectively. Red and blue solid lines are for the PC-PK1 and DD-ME2 calculations with the experimental occupation numbers, respectively. The gray areas show the statistical uncertainties.

FIG. 5. Same as Fig. 4, but the experimental results were obtained by using the SOG method.

which would be caused by an admixture of the isomer state in the beam [32]. If we adjust the systematic deviation of about 0.2 fm, the mentioned inconsistent issue for ^{22}Na in Ref. [44] is resolved.

The obtained matter density difference between ^{22}Ne and ^{24}Mg, $\rho(r)_{24\text{Mg}} - \rho(r)_{22\text{Ne}}$, is shown in Fig. 4, which is 2pF density model-dependent. In this work, only the surface density distributions were precisely determined, because the small-angle differential cross sections are not sensitive to deriving experimentally the central density profiles of nuclei. In general, the surface density range can be distinguished from the inner region by radial r at which the density falls to 90% of the central density [54]. Compared to ^{22}Ne, the densities in surface are higher for ^{24}Mg. In order to make it easier to understand, the density difference was convert into nucleon numbers via $N = 4\pi \sum \delta\rho(r)r^2 dr$. As shown in the insert in Fig. 4, about 2.63(22) extra nucleons are distributed in the radial r range from about 2 fm to 8 fm. According to the nucleon number conservation, if nucleon number increases in one place, decreases in the other region can be expected. Subtracting two valance protons, we can infer that about 0.63 nucleons in the inner r range from 0 fm to 2 fm are transferred into the surface region from ^{22}Ne to ^{24}Mg. Due to the decrease of the inner nucleons, the densities in the interior for ^{24}Mg are lower, compared to ^{22}Ne, see Fig. 4.

To check the effects of the 2pF density model, we also employed the sum-of-Gaussians (SOG) method to fit the differential cross sections. That is to say, the matter densities were described by the summation of the multi-Gaussian functions at arbitrary radius r_i range from 0 fm to the maximum radial radius $R_{\max}$. Since the number of data points N_0 are
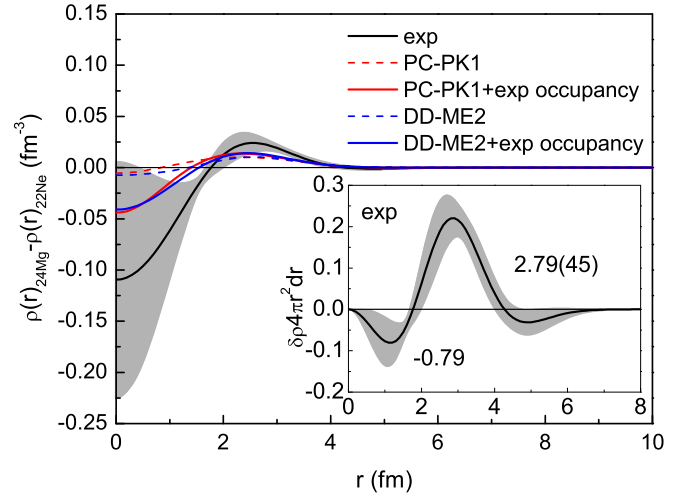
about 10 for the used differential cross sections, only five Gaussian functions were used to describe density distributions in this work. In the SOG analysis, the common width of the Gaussians γ and the maximum arbitrary radii $R_{\max}$ were fixed to be 1.4 fm and 4 fm, respectively. More details on the SOG analysis see Ref. [11]. Compared to the result based on the 2pF density model, as shown in Fig. 5, a similar conclusion was obtained.

Nucleon rearrangement directly reflects the variation of occupation numbers. The single-particle occupation numbers of the surface states for ^{22}Ne and ^{24}Mg were determined by direct reactions with the French and MacFarlane's sum rules in Ref. [22]. The reported nucleon occupation numbers of the $1d_{5/2}$, $2s_{1/2}$, and $1d_{3/2}$ orbitals are 4.5, 1.5, and 0.0 for ^{22}Ne, and 5.95, 0.34, and 1.72 for ^{24}Mg [22], respectively. They are the sum of the neutron and proton occupation numbers on corresponding orbitals. The nucleons of the $1d$ orbital are distributed in surface. However, the nucleon density distribution of the $2s$ orbital has two peaks, one is in the interior and the other one is in the surface of nuclei. Thus, the changes of the nucleon occupation numbers of the $2s_{1/2}$ orbitals from 1.5 for ^{22}Ne to 0.34 for ^{24}Mg would result in density decreasing in interior. As a result, the inner density in ^{24}Mg becomes lower. The nucleon rearrangement of the $2s_{1/2}$ orbital can explain our density difference.

Theoretically, the influences of single-particle structure on density distributions were investigated by the mean-field models [55–58]. In this work, the relativistic Hartree-Bogoliubov (RHB) with the DD-ME2 [59] and PC-PK1 interactions [60] were used to quantitatively calculate the density differences. The predicted nucleon occupation numbers of the $2s_{1/2}$ orbital by the DD-ME2 and PC-PK1 interactions are 0.11 and 0.13 for ^{22}Ne, and 0.09 and 0.10 for ^{24}Mg, respectively. Compared to the experimental occupation numbers [22], they are very small. As shown in Fig. 4, the calculations with the experimental occupation numbers describe the trend of the density difference between ^{22}Ne and ^{24}Mg better than the predicted occupation numbers. In particular, the calculated matter

density for ^{24}Mg with the experimental occupation numbers [22] shows a lower density in the interior, which is different from the distribution of ^{22}Ne, see Figs. 2 and 3. This indicates that ^{24}Mg may have a bubble structure in interior. However, due to the reported occupation numbers without errors [22], the effect of occupation number uncertainties on the calculated densities can not be studied. Otherwise, the correlations beyond the mean field also can modify the density distributions [61]. As a result, theoretical calculations with precise occupation numbers and appropriate correlations beyond the mean field [61] are helpful to further confirm the bubble structure in ^{24}Mg.

IV. SUMMARY

We extracted the matter density distributions of ^{20,22}Ne and ^{24,26}Mg from the reported small-angle differential cross sections of proton elastic scattering at 0.8 GeV by using the Glauber model. Based on the two-parameter Fermi density model, the obtained matter radii are 2.891(52) fm, 2.895(104) fm, 2.935(20) fm, and 2.946(21) fm for ^{20}Ne, ^{22}Ne, ^{24}Mg, and ^{26}Mg, respectively. The matter density difference between ^{22}Ne and ^{24}Mg was discussed. Combined with the experimental occupation numbers, the relativistic Hartree-Bogoliubov (RHB) calculations with the DD-ME2 and PC-PK1 interactions describe the trend of the density difference, and suggest that there may be a bubble structure in ^{24}Mg.

ACKNOWLEDGMENTS

[1] I. Tanihata, H. Savajols, and R. Kanungo, Prog. Part. Nucl. Phys. **68**, 215 (2013).

[2] P. Egelhof, Prog. Part. Nucl. Phys. **46**, 307 (2001).

[3] H. Sakaguchi and J. Zenihiro, Prog. Part. Nucl. Phys. **97**, 1 (2017).

[4] B. A. Li, L. W. Chen, and C. M. Ko, Phys. Rep. **464**, 113 (2008).

[5] J. T. Zhang, X. L. Tu, P. Sarriguren, K. Yue, Q. Zeng, Z. Y. Sun, M. Wang, Y. H. Zhang, X. H. Zhou, and Yu. A. Litvinov, Phys. Rev. C **104**, 034303 (2021).

[6] R. P. de Groote, J. Billowes, C. L. Binnersley, M. L. Bissell, T. E. Cocolios, T. Day Goodacre, G. J. Farooq-Smith, D. V. Fedorov, K. T. Flanagan, S. Franchoo *et al.*, Nat. Phys. **16**, 620 (2020).

[7] B. A. Marsh, T. Day Goodacre, S. Sels, Y. Tsunoda, B. Andel, A. N. Andreyev, N. A. Althubiti, D. Atanasov, A. E. Barzakh, J. Billowes *et al.*, Nat. Phys. **14**, 1163 (2018).

[8] I. Tanihata, H. Hamagaki, O. Hashimoto, Y. Shida, N. Yoshikawa, K. Sugimoto, O. Yamakawa, T. Kobayashi, and N. Takahashi, Phys. Rev. Lett. **55**, 2676 (1985).

[9] F. J. Fattoyev, J. Piekarewicz, and C. J. Horowitz, Phys. Rev. Lett. **120**, 172702 (2018).

[10] X. Liu, P. Egelhof, O. Kiselev, and M. Mutterer, Phys. Rev. C **104**, 034315 (2021).

[11] X. Liu, P. Egelhof, O. Kiselev, and M. Mutterer, Phys. Lett. B **809**, 135776 (2020).

[12] J. M. Cavedon, B. Frois, D. Goutte, M. Huet, P. Leconte, C. N. Papanicolas, X. H. Phan, S. K. Platchkov, S. Williamson, W. Boeglin, and I. Sick, Phys. Rev. Lett. **49**, 978 (1982).

[13] L. Ray, G. W. Hoffmann, M. Barlett, J. McGill, J. Amann, G. Adams, G. Pauletta, M. Gazzaly, and G. S. Blanpied, Phys. Rev. C **23**, 828 (1981).

[14] G. Pauletta, G. Adams, M. M. Gazzaly, G. J. Igo, A. T. M. Wang, A. Rahbar, A. Wriekat, L. Ray, G. W. Hoffmann, M. Barlett *et al.*, Phys. Lett. B **106**, 470 (1981).

[15] B. A. Brown, S. E. Massen, and P. E. Hodgson, Phys. Lett. B **85**, 167 (1979).

[16] G.W. Hoffmann, G. S. Blanpied, W. R. Coker, R. P. Liljestrand, L. Ray, J. E. Spencer, H. A. Thiessen, N. M. Hintz, M. A. Oothoudt, T. S. Bauer *et al.*, Phys. Lett. B **76**, 383 (1978).

[17] R. Soundranayagam, A. Saha, K. K. Seth, C. W. de Jager, H. de Vries, H. Blok, and G. van der Steenhoven, Phys. Lett. B **212**, 13 (1988).

[18] M. Grasso, L. Gaudefroy, E. Khan, T. Nikšić, J. Piekarewicz, O. Sorlin, N. Van Giai, and D. Vretenar, Phys. Rev. C **79**, 034318 (2009).

[19] L. T. Phuc, N. Q. Hung, and N. Dinh Dang, Phys. Rev. C **97**, 024331 (2018).

[20] B. G. Todd-Rutel, J. Piekarewicz, and P. D. Cottle, Phys. Rev. C **69**, 021301(R) (2004).

[21] J. Wesseling, C. W. de Jager, L. Lapikás, H. de Vries, L. W. Fagg, M. N. Harakeh, N. Kalantar-Nayestanaki, R. A. Lindgren, E. Moya De Guerra, and P. Sarriguren, Phys. Rev. C **55**, 2773 (1997).

[22] B. Castel, I. P. Johnstone, B. P. Singh, and J. C. Parikh, Nucl. Phys. A **157**, 137 (1970).

[23] Y. Chu, Z. Ren, Z. Wang, and T. Dong, Phys. Rev. C **82**, 024320 (2010).

[24] X. Campi and D. W. L. Sprung, Phys. Lett. B **46**, 291 (1973).

[25] H. A. Wilson, Phys. Rev. **69**, 538 (1946).

[26] A. Mutschler, A. Lemasson, O. Sorlin, D. Bazin, C. Borcea, R. Borcea, Z. Dombrádi, J.-P. Ebran, A. Gade, and H. Iwasaki, Nat. Phys. **13**, 152 (2017).

[27] S. Watanabe, K. Minomo, M. Shimada, S. Tagami, M. Kimura, M. Takechi, M. Fukuda, D. Nishimura, T. Suzuki, T. Matsumoto *et al.*, Phys. Rev. C **89**, 044610 (2014).

[28] M. Takechi, S. Suzuki, D. Nishimura, M. Fukuda, T. Ohtsubo, M. Nagashima, T. Suzuki, T. Yamaguchi, A. Ozawa, T. Moriguchi *et al.*, Phys. Rev. C **90**, 061305(R) (2014).

[29] M. Takechi, T. Ohtsubo, M. Fukuda, D. Nishimura, T. Kuboki, T. Suzuki, T. Yamaguchi, A. Ozawa, T. Moriguchi, H. Ooishi *et al.*, Phys. Lett. B **707**, 357 (2012).

[30] G. S. Blanpied, B. G. Ritchie, M. L. Barlett, G. W. Hoffmann, J. A. McGill, E. C. Milner, K. W. Jones, S. K. Nanda, and R. de Swiniarski, Phys. Rev. C **37**, 1987 (1988).

[31] G. S. Blanpied, B. G. Ritchie, M. L. Barlett, R. W. Fergerson, G. W. Hoffmann, J. A. McGill, and B. H. Wildenthal, Phys. Rev. C **38**, 2180 (1988).

[32] T. Suzuki, H. Geissel, O. Bochkarev, L. Chulkov, M. Golovkov, N. Fukunishi, D. Hirata, H. Irnich, Z. Janas, H. Keller *et al.*, Nucl. Phys. A **630**, 661 (1998).

[33] A. Ozawa, T. Suzuki, and I. Tanihata, Nucl. Phys. A **693**, 32 (2001).

[34] J. Zenihiro, H. Sakaguchi, S. Terashima, T. Uesaka, G. Hagen, M. Itoh, T. Murakami, Y. Nakatsugawa, T. Ohnishi, H. Sagawa *et al.*, arXiv:1810.11796 (2018).

[35] J. Zenihiro, H. Sakaguchi, T. Murakami, M. Yosoi, Y. Yasuda, S. Terashima, Y. Iwao, H. Takeda, M. Itoh, H. P. Yoshida *et al.*, Phys. Rev. C **82**, 044611 (2010).

[36] J. C. Zamora, T. Aumann, S. Bagchi, S. Bönig, M. Csatlós, I. Dillmann, C. Dimopoulou, P. Egelhof, V. Eremin, T. Furuno *et al.*, Phys. Rev. C **96**, 034617 (2017).

[37] D. Adhikari, H. Albataineh, D. Androic, K. Aniol, D. S. Armstrong, T. Averett, C. Ayerbe Gayoso, S. Barcus, V. Bellini, R. S. Beminiwattha *et al.*, Phys. Rev. Lett. **126**, 172502 (2021).

[38] A. V. Dobrovolsky, G. A. Korolev, S. Tang, G. D. Alkhazov, G. Colò, I. Dillmann, P. Egelhof, A. Estradé, F. Farinon, H. Geissel *et al.*, Nucl. Phys. A **1008**, 122154 (2021).

[39] G. D. Alkhazov, A. V. Dobrovolsky, P. Egelhof, H. Geissel, H. Irnich, A. V. Khanzadeev, G. A. Korolev, A. A. Lobodenko, G. Münzenberg, M. Mutterer *et al.*, Nucl. Phys. A **712**, 269 (2002).

[40] P. Egelhof, O. Kisselev, G. Münzenberg, S. R. Neumaier, and H. Weick, Phys. Scr. T **104**, 151 (2003).

[41] P. Egelhof, JPS Conf. Proc. **35**, 011002 (2021).

[42] K. Yue, J. T. Zhang, X. L. Tu, C. J. Shao, H. X. Li, P. Ma, B. Mei, X. C. Chen, Y. Y. Yang, X. Q. Liu *et al.*, Phys. Rev. C **100**, 054609 (2019).

[43] J. T. Zhang, K. Yue, H. X. Li, X. L. Tu, C. J. Shao, P. Ma, B. Mei, X. C. Chen, Y. Y. Yang, X. Q. Liu *et al.*, Nucl. Instrum. Meth. Phys. Res. A **948**, 162848 (2019).

[44] S. Sahoo, P. C. Srivastava, and T. Suzuki, Nucl. Phys. A **1032**, 122618 (2023).

[45] V. V. Zerkin and B. Pritychenko, Nucl. Instrum. Methods Phys. Res. A **888**, 31 (2018); https://www.nndc.bnl.gov/exfor/.

[46] G. D. Alkhazov, S. L. Belostotsky, and A. A. Vorobyov, Phys. Rep. **42**, 89 (1978).

[47] R. J. Glauber, in *Lectures in Theoretical Physics*, edited by W. E. Brittin and L. G. Dunham (Interscience, New York, 1959), Vol. 1, p. 315.

[48] G. D. Alkhazov, I. S. Novikov, and Yu. M. Shabelski, Int. J. Mod. Phys. E **20**, 583 (2011).

[49] J. Bystricky, C. Lechanoine-Leluc, and F. Lehar, J. Phys. France **48**, 199 (1987).

[50] H. De Vries, C. W. de jager, and C. de Vries, At. Data Nucl. Data Tables **36**, 495 (1987).

[51] Y. Huang, J. T. Zhang, Y. Kuang, J. Geng, X. L. Tu, K. Yue, W. H. Long, and Z. P. Li, Eur. Phys. J. A **59**, 4 (2023).

[52] A. Ong, J. C. Berengut, and V. V. Flambaum, Phys. Rev. C **82**, 014320 (2010).

[53] I. Angeli and K. P. Marinova, At. Data Nucl. Data Tables **99**, 69 (2013).

[54] G. A. Jones, Rep. Prog. Phys. **33**, 645 (1970).

[55] X. Y. Qu, H. Tong, and S. Q. Zhang, Phys. Rev. C **105**, 014326 (2022).

[56] M. Warda, M. Centelles, X. Viñas, and X. Roca-Maza, Phys. Rev. C **89**, 064302 (2014).

[57] W. A. Richter and B. A. Brown, Phys. Rev. C **67**, 034317 (2003).

[58] Soojae Im and J. Meng, Phys. Rev. C **61**, 064319 (2000).

[59] G. A. Lalazissis, T. Nikšić, D. Vretenar, and P. Ring, Phys. Rev. C **71**, 024312 (2005).

[60] P. W. Zhao, Z. P. Li, J. M. Yao, and J. Meng, Phys. Rev. C **82**, 054319 (2010).

[61] X. Y. Wu, J. M. Yao, and Z. P. Li, Phys. Rev. C **89**, 017304 (2014).